Experimental Mechanics (2015) 55:41–51
DOI 10.1007/s11340-014-9910-2

On the Uniaxial Ring Test of Tissue Engineered Constructs

Tarek Shazly · Alexander Rachev · Susan Lessner · William S. Argraves · Jahid Ferdous · Boran Zhou · Alexandra M. Moreira · Michael Sutton

Received: 6 November 2013 / Accepted: 9 June 2014 / Published online: 31 July 2014

Abstract Uniaxial tensile experiments are commonly used to evaluate the mechanical properties of engineered vascular tissues. We consider a typical uniaxial tensile experiment on a ring-shaped specimen and the corresponding theoretical framework within which the experimental data are processed when the sample undergoes a finite deformation. In some cases when the material is considered to be elastic, isotropic and incompressible, data obtained from a ring test can be processed to identify constitutive stress–strain relations via a strain energy function (SEF). Accurate identification of the SEF requires that the experimentally recorded deformations are acquired from a region sufficiently far away from the material-grip interface to minimize the confounding effects of friction and bending. Image-based tracking of surface markers provides a method by which the deformation of the ring sample can be locally recorded when subjected to uniaxial extension. We present an illustrative example of a uniaxial ring experiment on an engineered vascular tissue construct, and process the obtained data to identify the SEF. The SEF is used to perform a finite-element based computational simulation of the ring experiment, which is used to better understand the inherent errors and artifacts which may confound accurate data acquisition and correspondingly SEF identification. The obtained computational results provide guidance on the location of surface markers that facilitate accurate measure of local sample deformation for a range of materials.

Keywords Soft tissue · Uniaxial ring test · Marker tracking · Local strain · Constitutive model

T. Shazly (✉)
Biomedical Engineering (BME) Program in the Department of Mechanical Engineering (BME-ME), University of South Carolina (USC), Columbia, SC 29208, USA
e-mail: shazly@mailbox.sc.edu

A. Rachev
Biomedical Engineering Program, USC, Columbia, SC 29208, USA

S. Lessner
Cell and Developmental Biology, USC School of Medicine, Columbia, SC 29208, USA

W.S. Argraves
Cell and Developmental Biology, Department at the Medical University of South Carolina, Columbia, SC 29208, USA

J. Ferdous · B. Zhou · A.M. Moreira
BME Program, USC, Columbia, SC 29208, USA

M. Sutton
Department of Mechanical Engineering, USC, Columbia, SC 29208, USA

Introduction

Quantification of the mechanical properties of vascular tissue is essential for understanding the physiological function of arteries and for the design and fabrication of arterial substitutes to replace diseased vessels. Focusing on the development of tissue engineered arteries, it is important to obtain reliable and useful preliminary information about mechanical properties of tissue constructs immediately after fabrication and following mechanical conditioning in bioreactors. Moreover, because vascular cells are mechanosensitive and the process of neo-artery formation is governed by the local stress existing in the wall of the tissue engineered artery, there is a practical need to calculate the wall stress distribution with appropriate predictive mathematical models. Proposing such models necessitates a constitutive formulation of arterial tissue in the framework of soft tissue biomechanics. As a first step it is important to perform relatively simple mechanical experiments to quantify the material properties, while minimizing

errors and artifacts, and to process the recorded data towards formulation of reliable constitutive equations.

A uniaxial tensile experiment is among the simplest mechanical tests that can be performed on a specimen made of a solid material. In the case of materials that exhibit high stiffness, linear elasticity, mechanical isotropy, and undergo small deformations under applied loads, including metals and most plastics, results from uniaxial experiments are sufficient to characterize the material response in terms of continuum based mechanical descriptors such as Young's modulus and Poisson's ratio. Thus for this class of materials, uniaxial experiments allow formulation of general constitutive stress–strain relations that can be used for solving two-and three-dimensional boundary-value problems and obtaining predictive results of great utility in engineering practice. In contrast, uniaxial experiments performed on materials that undergo finite (large) deformations (e.g., soft tissues and tissue engineered constructs) are in general not sufficient to identify the constitutive stress–strain relations. Even so, uniaxial experiments on these materials can reveal descriptive and useful mechanical information, provided the recorded experimental data are correctly processed and analyzed.

Focusing on blood vessels and tissue engineered vascular constructs, uniaxial experiments are done using specific shaped specimens; rings, dumbbell-shaped specimens or specimens with helically-oriented fibres excised from tubular samples are commonly used [1–6]. Since most soft tissues, including vascular tissue, are mechanically anisotropic, their mechanical properties depend upon the direction of the applied forces [7]. Therefore careful specimen preparation for mechanical testing is necessary since the tissue excision process may influence the results obtained. For example, the anisotropy introduced by collagen fibers in the arterial wall produces disparate results in uniaxial tests depending on whether the excised specimens are oriented longitudinally or circumferentially relative to the vessel axis [8].

In this study, we consider acquisition and processing of data from a uniaxial tensile experiment on ring-shaped tissue constructs formed by self-adhering gelatin microcarriers cellularized with human endothelial cells (HUVECs) and human aortic smooth muscle cells (HASMCs) [9]. A particular focus is paid to the use of particle tracking techniques to identify the sample region in which the tissue experiences homogenous deformation. Under some reasonable assumptions a single invariant constitutive model is proposed. Finally, a finite element model that simulates the experimental methods is built to study the effects of tissue mechanical properties on regions of uniform strain distribution.

Uniaxial Test for Ring-Shaped Specimens

We consider a typical uniaxial tensile experiment and the corresponding theoretical framework within which the experimental data are processed. For cases involving quantification of the mechanical properties of blood vessels or tissue engineered vascular constructs in the circumferential direction, ring specimens are commonly used for uniaxial experiments [e.g. 2, 3]. A small ring is fabricated or excised from a tubular vessel and then mounted between two metallic arms. Before test initiation and acquisition of experimental data, the ring is preconditioned by applying several loading-unloading cycles to obtain a reproducible displacement-force curve as proposed in [7] and utilized in virtually all experimental tests on biological soft tissues [10]. Following preconditioning the ring is immediately subjected to monotonic uniaxial extension by applying displacement at low rates of 0.01 mm/s to 1 mm/s, and the tensile force F and the corresponding deformations of the ring are recorded [7]. In the classical ring experiment, the distance between the arms is recorded as shown in (Fig. 1. The global stretch ratio in the circumferential direction is calculated as $\lambda_{global}=(l+\pi R)/(L+\pi R)$, where L and l are the undeformed and deformed distances between arms, respectively, and R is the radius of the cylindrical loading arms [10].

In fact due to bending and friction at the arms, the stretching of the sample is not uniform and λ_{global} represents an averaged measure of the stretch ratio along the ring circumference. In general the measurement of local strains is based on tracking the change in distance between closely spaced markers that are affixed to the specimen during deformation. Different image-based techniques of tracking have been used, such as video cameras, x-ray, and magnetic resonance imaging [e.g. 11–14]. The local stretch ratio in the vicinity of a point located on the straight part of the ring is calculated as $\lambda_{local}=s/S$, where s and S are the distances between two markers around the point of interest in the deformed and undeformed configurations, respectively (Fig. 1). An extension of this approach is to apply a nominally random pattern to the ring specimen and use subsets from the

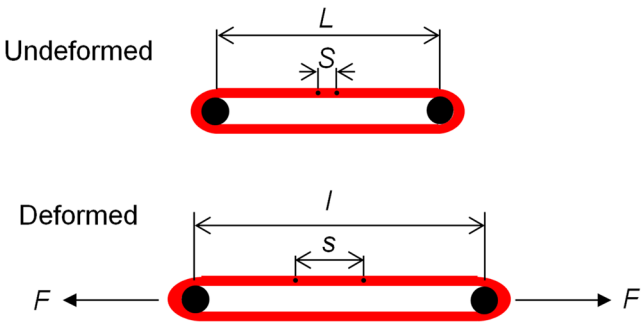

Fig. 1 Schematic of the uniaxial ring experiment. Lengths L and S refer to the undeformed configuration, and l and s refer to a deformed configuration induced by the application of uniaxial force F

pattern as the markers. By tracking subsets from the pattern along the entire length of the ring specimen during mechanical loading, investigators can obtain the variations in strain that occur (a) near the posts and (b) in the transition region between the post and the straight sections of the specimen by using digital image correlation methods [e.g. 15–22]. If there is a potential for significant deformations out of plane, 3-D digital image correlation is often used to improve measurement accuracy [e.g. 23, 24].

Assuming that the material is incompressible, which is virtually true for most soft biological tissue due to high water content, the Cauchy stress (force per unit deformed area) is calculated as $\sigma=(F\lambda)/(2BH)$, where B and H are undeformed specimen width and thickness. Thus, the selection of either λ_{local} or λ_{global} will influence the value of stress calculated for each deformed state.

Monotonic Tensile Experiments

Monotonic tensile experiments provide useful information on how the mechanical properties of native vessels are affected by factors such as location, aging and pharmacological treatment and on how engineered vascular constructs are influenced by manufacturing protocol, composition, mechanical and chemical conditioning and storage. Moreover, as discussed below, the results from ring experiments can be used to identify the constitutive stress–strain relations for a special class of elastic materials. The shortcomings of uniaxial experiments on vascular tissue, and in particular the monotonic tensile experiments, are the facts that they do not mimic the load conditions that exist in-vivo and do not account for the possible existence of residual strains in tubular specimens in the load-free state.

If monotonic tensile experiments are conducted to describe the mechanical behavior of a material and enable comparison among various samples, consistent processing of data in terms of either local or global stretch ratios is likely equally valid. However, if experimental data are to be used to identify constitutive stress–strain relations, local measures of the stretch ratio taken in the central portion of the ring specimen should be used to minimize the influence of friction, local compression, and bending due to contact with the arms. In the case of vascular tissue, variation of strains due to material non-homogeneity can be neglected due to the insignificant change in structure and composition along the ring circumference in all native blood vessels except the aorta [25].

Based on the Saint-Venant's Principle [26] that states the effects of two different but statically equivalent loads become virtually identical at sufficiently large distances from the point of application, it is generally recommended to calculate the local strains at locations close to the middle of the straight portion of the ring. However precise identification of the size of the region over which the local stretch ratios have a near uniform distribution and how the size of that region varies with sample extension and material stiffness remain open questions that are addressed in this study.

One-Dimensional Constitutive Stress–Strain Relations

Constitutive equations describe the mechanical behavior of solids in terms of relations between continuum-based categories such as strains and stresses. An elastic solid is incapable of dissipating energy and all the mechanical work done during loading is recoverable. Restricting to the class of elastic solids for which the stress–strain relations are given in an explicit and single-valued form, elasticity implies the existence of a strain energy function (SEF), which is a function of the components of the strain tensor. If the material is mechanically isotropic and incompressible, the SEF is a function of the first and second invariant of the Green strain tensor, i.e. $W=W(I_1,I_2)$ [7]. As was shown in the theory of finite elasticity, the one-dimensional constitutive equation that relates the only non-zero Cauchy stress and corresponding stretch ratios along the direction of stress is given by the relation [10, 27]

$$\sigma = \left(\lambda^2 - \frac{1}{\lambda}\right)\left(\varphi(I_1,I_2) - \frac{1}{\lambda_1}\psi(I_1,I_2)\right) \tag{1}$$

where

$$\varphi(I_1,I_2) = 2\frac{\partial W}{\partial I_1}\ , \qquad \psi(I_1,I_2) = -2\frac{\partial W}{\partial I_2} \tag{2}$$

are the "response functions" and the strain invariants are.

$$I_1 = {\lambda_1}^2 + \frac{2}{\lambda_1}, \qquad I_2 = 2\lambda_1 + \frac{1}{{\lambda_1}^2} \tag{3}$$

The recorded data from a uniaxial tensile experiment allows investigators to calculate the Cauchy stress and the stretch ratio at each deformed state and provide one functional relation between them. However, this information is not sufficient to identify both of the response functions, which are potentially unknown functions of the strain invariants. Therefore quantification of the SEF for an isotropic incompressible elastic material requires processing data from at least a two-dimensional mechanical experiment. However, theoretically there exist particular cases when the results from a monotonic tensile ring experiment can be used to quantify the SEF. This is possible if both of the response functions are constants for any deformation (Mooney-Rivlin material) or if one is zero. So far, no biological or synthetic material has been identified for which $\varphi=0$. On the contrary, soft tissues with structures that contain long chain molecules might have a SEF which depends solely on the first strain invariant, i.e. $W=$

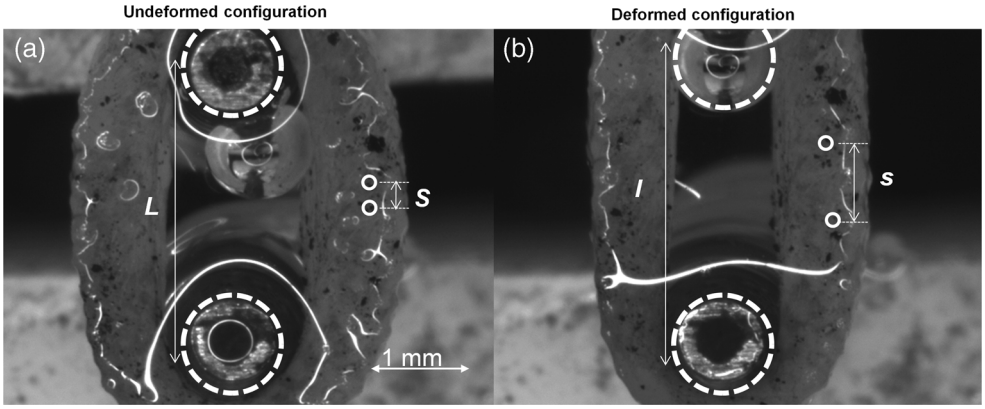

Fig. 2 Acquired images from a uniaxial ring experiment on an engineering vascular construct. The distance between markers contained within the central region of the sample longitudinal *axis* was measured in the undeformed (**a**) and deformed (**b**) states to facilitate calculation of a local stretch ratio. The scale bar refers to both images

$W(I_1)$ and hence $\psi=0$. Typical representatives of that class of solids, termed Neo-Hookean materials, are elastin and rubber for which

$$W=\frac{\mu}{2}(I_1-3),$$

where μ is a material constant. A more general analytical form of an exponential-type SEF was proposed for engineered and native vascular tissue [7, 10] and polyvinyl alcohol hydrogel-based synthetic materials [28, 29] as follows

$$W=\frac{c}{a}[\exp[a\ \ (I_1-3)]-1] \tag{4}$$

where c and a are material constants.

If $W=W(I_1)$, the data from a uniaxial experiment allow for determining both the analytical form and the material constants of the SEF. Setting $\psi=0$ in equation. (1) and accounting for Eqs. (2) and (3) yield.

$$\frac{\partial W}{\partial I_1}=\frac{\sigma\lambda}{2\left(\lambda^3-1\right)} \tag{5}$$

Because the values of both the stress σ and stretch ratio λ are calculated from recorded changes in specimen length and applied tensile force, equations. (3) and (5) allow calculating the corresponding values of $\partial W/\partial I_1$ and I_1 for each recorded deformed state of the ring. A representative point n that has coordinates $(\partial W/\partial I_1)_n$ and $(I_1)_n$ can be plotted in the $I_1-\partial W/\partial I_1$ plane for each (n^{th}) experimental state. The best fit analytical approximation of all representative points, say $(\partial W/\partial I_1)=\mathcal{J}(I_1)$, yields a differential equation for the unknown function $W=W(I_1)$. The integral of this equation, with the condition that $I_1=3$ and $W=0$ when no deformation occurs, yields the SEF that describes the mechanical properties of the tissue under study within the model of an elastic solid.

In particular, when the anticipated analytical form of SEF is of exponential type as given by equation. (4), it is more convenient to plot the representative points on a semi-logarithmic scale. If linear regression yields a satisfactory approximation of representative points, the differential equation is $\ln(\partial W/\partial I_1)=A+KI_1$, where A and K are the calculated linear regression coefficients. Then the SEF has the form given by equation. (4) with $a=A$ and $c=\exp(3A+K)$ as shown in [28, 29]. Determining the SEF then allows for formulation of two- and three-dimensional constitutive equations that can be used for solving different boundary value problems, for instance simultaneous inflation and axial extension of a thick-walled tube. Comparison between theoretical solutions and

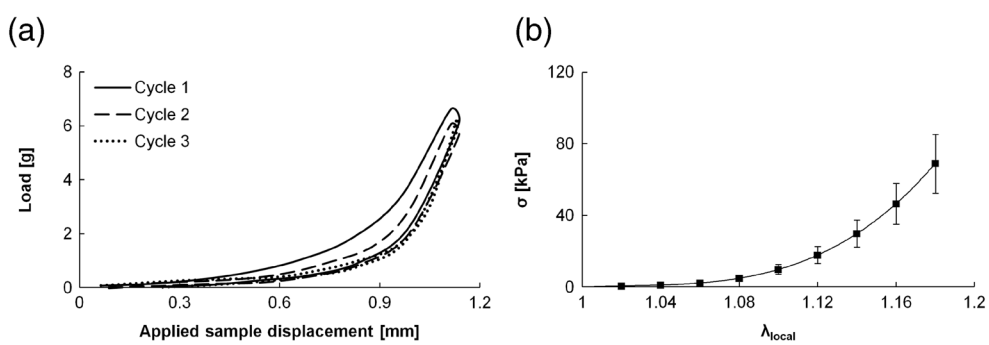

Fig. 3 Experimental preconditioning and data obtained from a uniaxial ring test. (**a**) Ring constructs were preconditioned with three loading-unloading cycles to obtain a reproducible elastic response. (**b**) Immediately following preconditioning, an identical fourth cycle was performed, and loading data processed to develop stress-stretch relations. Error bars represent the standard deviation of measurements made on four samples

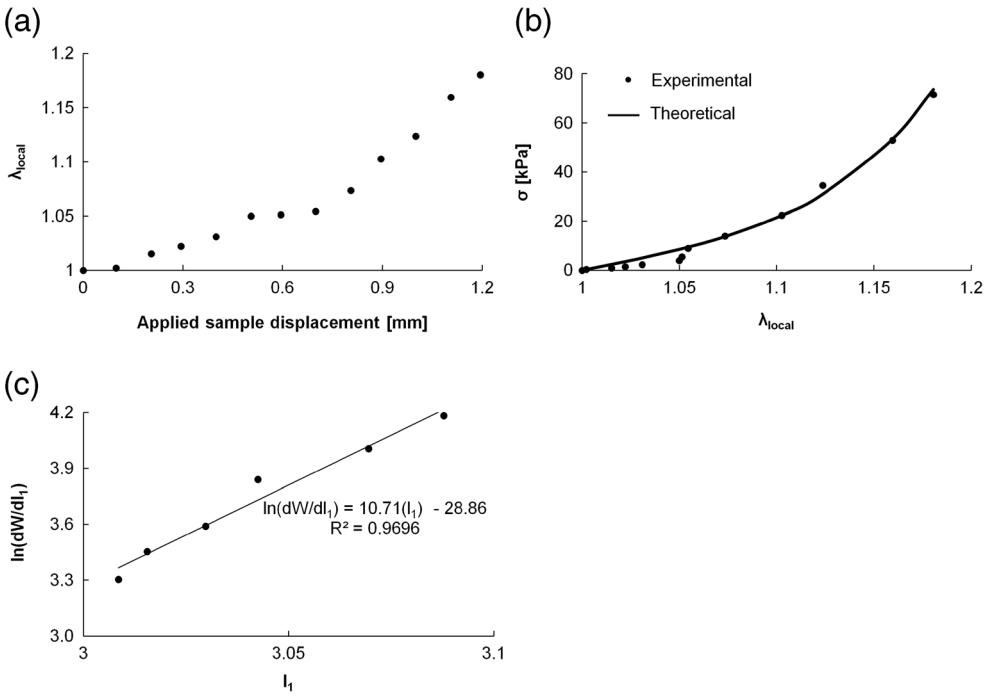

Fig. 4 Experimental and theoretical results obtained from a uniaxial ring experiment on engineering vascular constructs. (**a**) Experimental values of the local stretch ratio over the range of applied displacements from a representative material sample. (**b**) Cauchy stress-stretch relations generated from processing of experimental data (*points*), as well as corresponding theoretical relations (*line*) generated with an exponential-type SEF. (**c**) Experimental data exhibited a linear relationship in the $\ln I_1 - \partial W/\partial I_1$ plane, enabling identification of material parameters for the exponential-type SEF via linear regression

data from corresponding experiments can validate the identified SEF.

In the general case, the mechanical properties of soft biological tissue are determined from data acquired with at least bi-axial mechanical experimentation. In the past, SEFs were quantified from the requirement for a best fit to experimental data (phenomenological approach), with no account for the specific tissue structure and composition. However, most biological tissues are composed of load-bearing constituents with individual spatial organization and mechanical properties. Therefore, in recent studies the analytical forms of the SEF were selected to account for the structure of the tissue (structure-motivated approach) [e.g. 30, 31] or by making use of the theory of constrained mixtures (structure-based approach) [e.g. 32]. In the last case, the SEF is a sum of the individual SEFs of the tissue constituents weighted by their mass fractions.

Uniaxial Ring Test of an Engineered Vascular Construct and Constitutive Material Formulation

A representative material for vascular tissue engineering applications was synthesized and mechanically characterized with a ring test. Ring-shaped samples composed of fused gelatin CultiSpher-G microcarrier beads (Percell Biolytica, Astorp, Sweden) laden with human umbilical vein endothelial cells (HUVECs, Lonza; Basel, Switzerland) and human aortic smooth muscle cells (HASMCs, Lonza) were synthesized as previously described [9]. Samples were formed following microcarrier fusion within ring-shaped agarose molds, which occurred over a twelve day culture period.

To perform mechanical testing, rings were removed from culture and immediately secured onto horizontally-oriented 25 gauge cannulas mounted to the upper and lower arms of a uniaxial mechanical tester (Bose Enduratec 3,200) (Fig. 2). Each ring sample (N=4) was kept hydrated with culture medium prior to testing and also while being mechanically preconditioned, which consisted of three tensile displacement cycles up to 1.2 mm at a displacement rate of 0.01 mm/s (Fig. 3a). An identical fourth cycle was then immediately performed, during which load data (50 points/s) was recorded by system software (Bose Wintest). A maximum arm displacement of 1.2 mm was selected to cover the physiologically-relevant strain range for arterial substitutes [7].

To enable measurement of local strain, blue tissue marking dye was applied to the ring surfaces by a fine tip applicator to create a speckle pattern, yielding a relatively sparse random pattern that is clearly visible throughout the test (Fig. 2). Due to the sparsity of the speckle pattern, we identified two separate speckles located within 0.5 mm of the center of the straight portion of the undeformed ring specimen. A typical pair of speckles used in these studies is shown in (Fig. 2.) Once the speckles are identified, the distance between them at each experimental state was measured using what is essentially a marker-tracking approach. Since the marker-tracking method used is 2-D in nature, it must be noted that (a) the speckles selected for the measurements were located near the apex of the curved ring specimen surface and (b) speckle motions were nearly vertical, with minimal rotation of the ring specimen. Thus, out of plane motions were negligible during the

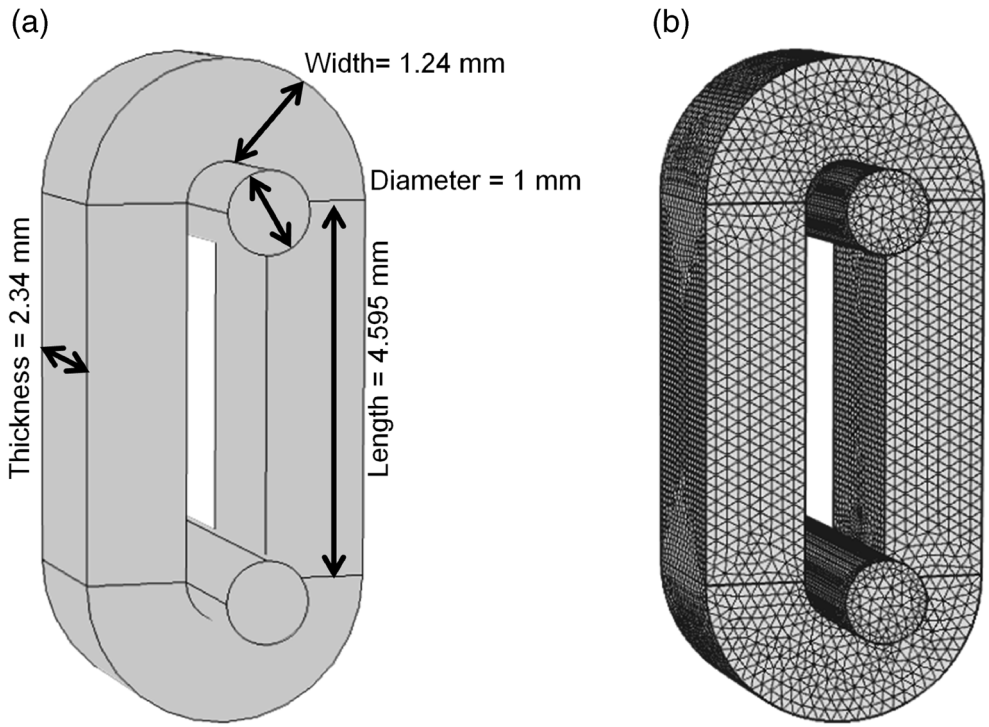

Fig. 5 Geometry for developed computational model. (**a**) The model geometry contains a ring and two arms, with dimensions and configuration reflective of the presented representative uniaxial ring experiment. (**b**) An adaptive scheme was used to generate a mesh of the model geometry

experiment, supporting the assumption that throughout the region of interest, the sample is in a state of true bi-axial deformation. A series of surface images was captured throughout testing using a Nikon SMZ-U light microscope and a Q-Imaging camera. The distance between markers at various experimental states was determined by post-processing of the acquired images with ImagePro 5.1. In this process, an edge/vertex on each marker was identified on consecutive images, and the distance in pixels between the positions on both markers was determined. Here, the average of three independent estimates was used to define the local stretch ratio for each experimental state. The estimated standard deviation in stretch ratio using this approach is ~1.004 for our imaging setup. The average stress-stretch response generated via image-based measurements of the ring constructs is given in (Fig. 3b).

Recorded mechanical data for a representative ring, namely the applied sample displacement, vertical distance between select markers, and axial force at each experimental state, were processed to generate plots of the local stretch ratio over the range of applied sample displacement (Fig. 4a) and the corresponding Cauchy stress-local stretch relation (Fig. 4b).

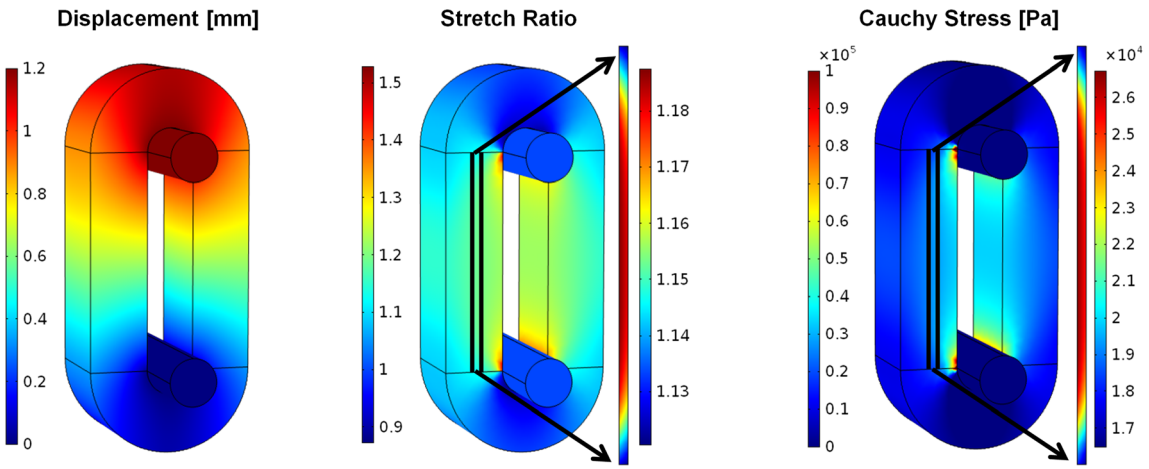

Fig. 6 Surface plots of simulation results. Simulation results were processed to yield the displacement, stretch ratio, and Cauchy stress in the sample longitudinal direction throughout the ring (applied upper arm displacement=1.2 mm in all surface plots)

Ring constructs exhibited a nonlinear elastic response, generally supporting the application of the proposed exponential-type SEF as a material mechanical model.

The experimental data were processed to identify material constants (a and c) in (equation. 4) as described above. As an intermediate step, the coefficients of a linear regression between ln (dW/dI_1) versus I_1 were determined (Fig. 4c). The relationship is virtually linear, with transformation of the regression coefficients yielding a=10.71 and c=26.31 kPa in this particular case.

Using the identified SEF and the corresponding one-dimensional constitutive equation (equation. 1), a theoretical stress-stretch relation was calculated and compared to experimental data (Fig. 3b). Very good correlation exists between experimental and theoretical results (R >0.97), providing further support for application of (equation. 4) to model the mechanical behavior of engineering vascular constructs. However, this correlation in no way demonstrates the predictive power of the identified SEF, which can only be achieved via accurate prediction of the mechanical response of the same material under different mechanical loads or with different geometry. At the present stage we have not performed validation studies, such as inflation tests on tubular specimens. Despite this fact, there are good reasons to expect that SEF given by equation. (4) is an adequate constitutive model of the fabricated tissue. We reiterate that the derivation of equation. (4) is based on two fundamental assumptions, namely that the material can be considered as an isotropic elastic solid and the corresponding SEF is solely a function of the first strain invariant. The following arguments indirectly support these suppositions.

The ring-shaped tissue constructs are formed by cellularized self-adhering gelatin microcarriers after a short-term culture period (12 days). Due to the method of fabrication [9] it is logical to posit that the material initially exhibits mechanical isotropy. Gelatin itself has a long-chained structure that includes a mixture of single and multi-stranded polypeptides with individual chains containing 50–1,000 amino acid residues. A long-chained structure is typical also for some synthetic materials such as polyvinyl alcohol (PVA) hydrogels. As referenced in the previous section, the SEF determined from data of a uniaxial extension on samples made of a PVA-based biomaterial has the analytical form given by equation. (4). Using the solution for a finite inflation a long thick-walled tube [27], the determined SEF was used to predict the mechanical response of a pressurized tube made of the PVA hydrogel kept at constant length [28, 29]. Good correlation (r=0.99) was noted between the theoretical predictions and experimental data, verifying the proposed SEF. Similarity in structure between PVA hydrogel and the material considered in this study suggests validity of the proposed SEF given by equation. (4).

Another supporting argument is the notion that while the gelatin provides a temporary scaffold for cellular adhesion and a capacity for ring constructs to bear load prior to extracellular matrix elaboration, incorporated cells produce a significant amount of elastin over 12 days of culture, which leads to a progressive stiffening of the fabricated constructs [9]. It has gained acceptance that elastin can be considered as neo-Hookean material which is a particular case of elastic solid for which the SEF depends solely on the first strain invariant [33, 31]. Of course further studies are needed to specify precisely the conditions under which the SEF given by equation. (4) represents a relevant constitutive model for the fabricated arterial tissue.

With progression of culture the smooth muscle cells produce collagen fibers and the construct material exhibits orthotropic rather than isotropic mechanical properties. Data from a single uniaxial tensile experiment are then not sufficient for SEF identification. However and though not often used, data from two uniaxial tensile experiments on strips excised in direction of the main axes of orthotropy can be processed to quantify the SEF [e.g. 34–36]. The major shortcoming of this approach is that most of the data used for

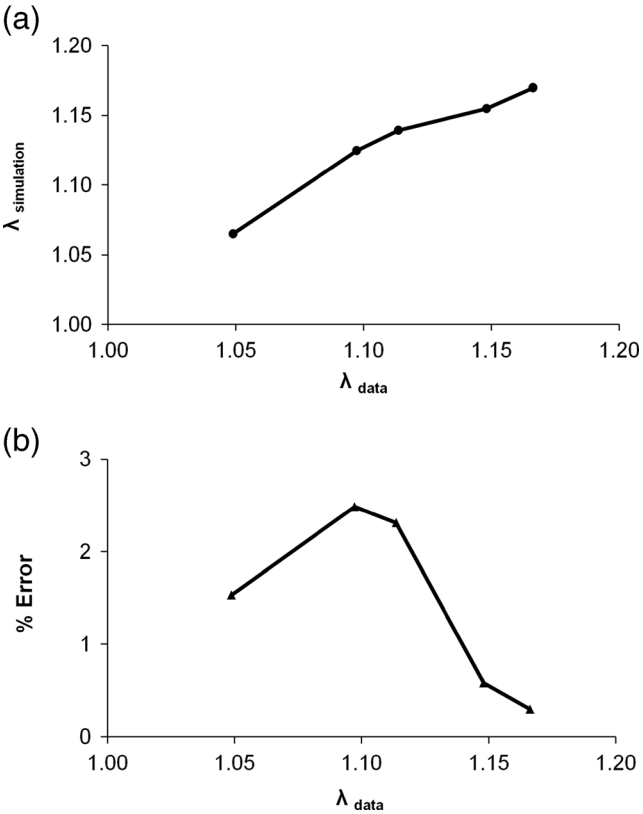

Fig. 7 Validation of simulation results. (**a**) A comparison of the simulated and experimentally recorded stretch ratio in the center of the sample at equivalent arm displacements. (**b**) The percent error between simulated and experimentally measured stretch ratios $\left(100 \times \frac{\lambda_{simulated}-\lambda_{data}}{\lambda_{data}}\right)$ ranges from 0.29 to 2.48 % over the examined arm displacements, providing support for the accuracy of the developed model

identification of material constants do not belong to the domain of strains experienced by arterial tissue under physiological load.

Computational Study of the Effects of Tissue Mechanical Properties on Regions of Uniform Strain

For accurate calculation of λ_{local}, tracked markers at each experimental state should be contained within a sample region that is experiencing near uniform strain. A finite-element model was constructed with a commercial software package (COMSOL Multiphysics^{TM}) to quantify the variation of strain along the sample length in a simulated ring test. The model geometry consists of two cylindrical arms and a ring, with dimensions and positions that reflect the reference configuration in the representative uniaxial ring experiment on engineered vascular tissue described above (Fig. 5a). Idealized semicircular contact between the arms and the ring was assumed for the reference state. The arms were defined as linear elastic materials with steel-like material properties (Young's modulus=200 GPa, Poisson's ratio=0.33, density=7,850 kg/m^3), while the ring was defined with (equatio. 4) and the experimentally determined material constants. An adaptive meshing scheme using linear tetrahedral elements was applied to all domains, resulting in a maximum density of elements around curved portions of the geometry (Fig. 5b).

Model boundary conditions consisted of holding the lower arm at a fixed position, and prescribing a vertical displacement to the upper arm. A frictionless contact was assumed between the ring specimen and the arms. All surfaces of the ring were assigned as traction-free. A built-in nonlinear stationary solver (GMRES) was used to calculate mesh displacement as a result of the prescribed boundary conditions. Post-processing of the simulation results was performed to yield the displacement, stretch ratio, and Cauchy stress in the sample longitudinal direction throughout the deformed ring volume (Fig. 6). The computational solution was considered mesh-independent when the relative change in peak ring stretch ratio under a prescribed arm displacement of 1 mm was less than 0.1 % following iterative mesh refinement. In this case, mesh independence was achieved with a maximum element size of 0.1 mm and 344,816 total mesh elements as depicted in (Fig. 5b).

The developed simulation was validated via comparison of the predicted local stretch ratio in the central portion of the ring to the experimentally recorded value (Fig. 7a). Over the range of applied arms displacements, the percent difference between simulated and experimentally recorded local stretch ratios was less than

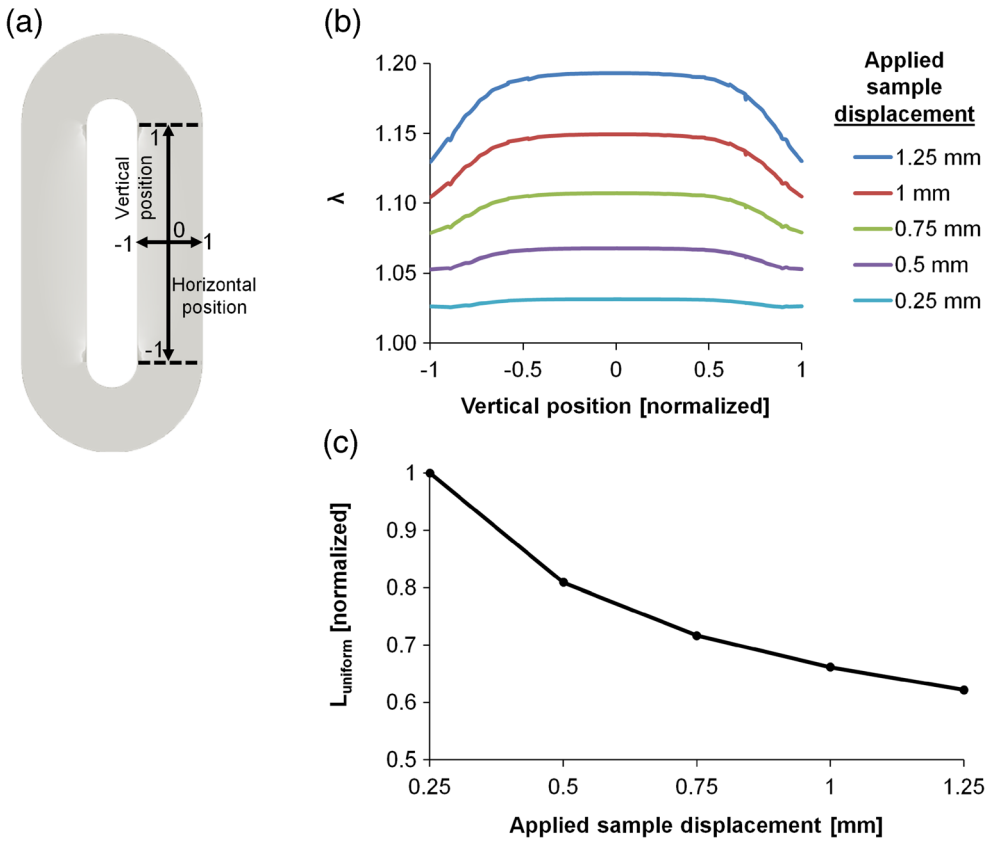

Fig. 8 Predicted variation in stretch ratio along the sample length. (**a**) Normalized horizontal and vertical positions were defined relative to the sample center. (**b**) The stretch ratio along the central sample longitudinal axis (horizontal position=0, vertical position=−1 to 1) exhibited variation at all levels of prescribed displacement, with lower values near the arms. (**c**) The normalized sample length experiencing near uniform strain (±1 % of central value, termed $L_{uniform}$) exhibited an inverse relationship to the magnitude of the applied sample displacement

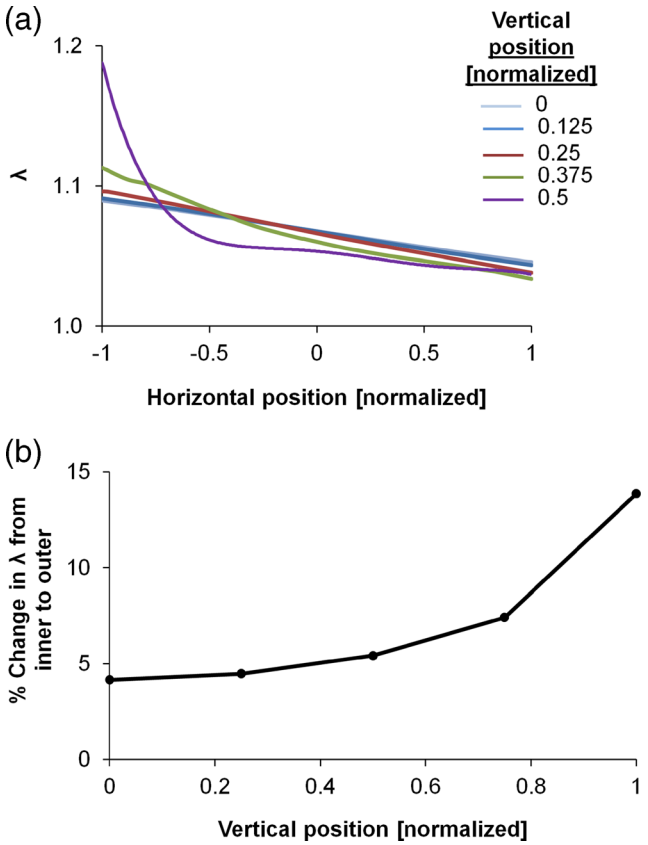

Fig. 9 Predicted variation in stretch ratio along the sample width. (**a**) The stretch ratio at horizontal positions across the sample width ranged from a maximal value at the inner surface to a minimal value at the outer surface at all vertical positions (applied displacement=0.5 mm). (**b**) The percent change in stretch ratio from the inner to outer surface $\left(100 \times \frac{\lambda_{inner}-\lambda_{outer}}{\lambda_{avg}}\right)$ was minimal at the sample central vertical position

3 % (Fig. 7b), indicating acceptable accuracy for the developed computational model.

A series of line plots corresponding to sample displacements over the range of 0.25 mm to 1.5 mm were used to determine the variation in stretch ratio on the sample surface (where tracker markers would be located), specifically along the central sample longitudinal axis (normalized horizontal position=0, vertical position={−1 to 1}) (Fig. 8a). At all levels of prescribed displacement, the stretch ratio is smaller near the arms compared to the value in the central sample region (Fig. 8b). Line plot data were used to determine the fraction of the undeformed central longitudinal axis over which the stretch ratio was within 1 % of the central value, termed $L_{uniform}$. An inverse relation was found between the magnitude of the prescribed displacement and $L_{uniform}$, suggesting that the region over which stretch ratio is constant in a ring test will depend on the applied loading conditions (Fig. 8c). Therefore, in the course of a monotonic tensile experiment, it is possible that some markers close to the arm transition between sample regions that experience near uniform and non-uniform stretch. The use of these markers to calculate λ_{local} would confound the identification of constitutive material properties, and thus should be avoided.

Simulation results were further used to examine the horizontal variation in stretch ratio at various vertical positions along the sample length. At all vertical positions, the stretch ratio monotonically decreases from the sample inner surface to the outer sample surface (Fig. 9a). The magnitude of the variation was expressed as a percent difference between the stretch ratio at the inner and outer surface, and is minimal at the vertical center of the sample (Fig. 9b). A plausible explanation of this discrepancy is the manner by which the load is transmitted to the tissue due to the arms-specimen interaction. The force generated by the displacement of the arms is distributed into two parts each applied eccentrically with respect to the center of gravity of the cross-sectional area of the load-bearing tissue and therefore being equivalent to a tensile force and a bending moment. As a result, the tensile stress and respectively the stretch ratio at the inner horizontal location are larger as compared to the stress and stretch ratio at the outer location. Obviously this effect is less pronounced when the thickness of the specimen is smaller. The theorical model is based on the assumption that there is no friction between the specimen and the metallic arms which is consistent with above explanation. Thus, for accurate measurement of local stretch using marker tracking, markers should be located not only

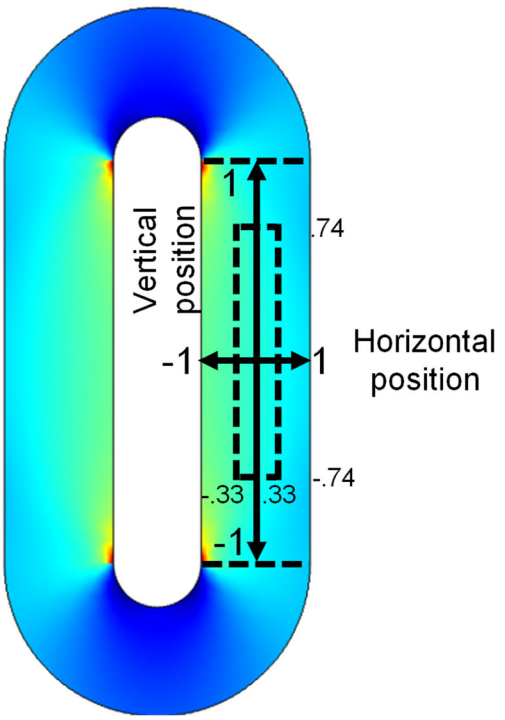

Fig. 10 Predicted sample region of near uniform stretch ratio. Within the indicated sample surface area (*dashed box*), the stretch ratio varies by less than 1 % at an arm displacement of 0.5 mm

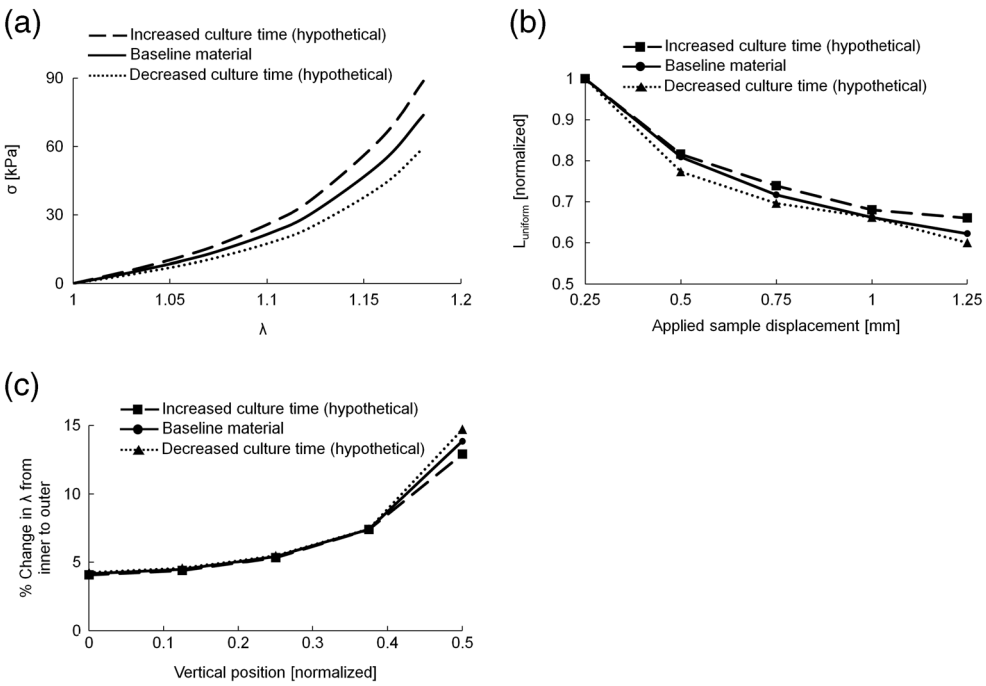

Fig. 11 Predicted variation in stretch ratio for a range of materials. (**a**) Comparatively stiff and compliant materials were considered for computational studies, which could reflect constructs cultured for different time periods. (**b**) The normalized sample length experiencing near uniform strain (±1 % of central value, termed $L_{uniform}$) and (**c**) the percent change in stretch ratio from the inner to outer surface $\left(100 \times \frac{\lambda_{inner}-\lambda_{outer}}{\lambda_{avg}}\right)$ were both largely insensitive to material properties over the examined range

within the central sample region, but should also have near equivalent horizontal positions. Simulation results for an applied arm displacement of 0.5 mm were processed to identify a surface region over which the stretch ratio varied by less than 1 % from the central value (Fig. 10). At this experimental state, approximately 25 % of the surface area on the straightened-out ring segment is experiencing a near uniform stretch ratio. Taken together, simulation results imply that the size of this region will diminish with increasing arm displacement, which should be considered in the performance and analysis of a uniaxial ring test on soft tissue.

Additional computational studies were performed to assess the applicability of the obtained results for a hypothetical material that is comparatively stiff due to increased culture time, with material parameter values of a=10.77 and c=31.50 kPa, as well as one which is comparatively compliant due to decreased culture time, with a=10.64 and c=21.32 kPa (Fig. 11a). These scenarios thus represent tissue constructs fabricated by the same methodology but cultured for different periods of time, albeit with retention of the analytical form of SEF given by equation. (4) and adherence to its underlying assumptions. Analogous analyses of these materials demonstrate that the computational predictions of regions of uniform strain are largely independent of material properties over the examined range, suggesting that the provided guidelines for the ring test have a general applicability to engineered arterial tissue (Figs. 11b and C).

Conclusion

The uniaxial mechanical response of engineered and synthetic vascular tissues is typically characterized with a ring test, and is valuable for providing descriptive mechanical data to elucidate how various factors impact material properties. For some special cases of mechanically isotropic materials, data from the ring experiment can be processed to identify the constitutive stress–strain relations that can be used for solving 2D and 3D boundary-value problems. The solutions of these problems predict the material mechanical response under conditions that deviate from the performed uniaxial ring experiment, i.e. for samples with different geometries and experiencing different loading. In order to minimize confounding factors due to sample contact with the arms and enable accurate identification of material-specific mechanical parameters in the ring test, investigators should assess the stress-stretch response based on a local measurement of stretch ratio taken near the center of the straightened-out portion of the specimen. Moreover, provisions should be made to ensure that markers used for calculation of the local stretch ratio remain within a region of uniformity throughout monotonic extension, as the relative size of this region will diminish with increasing deformation. Computational models can provide a tool for estimating the region of uniform stretch ratio in the ring experiment, and thus provide guidance for the development of accurate testing protocols for identification of constitutive material parameters.

References

1. Azuma T, Hasegawa M (1971) A rheological approach to the architecture of arterial walls. Jpn J Physiol 21(1):27
2. Cox RH (1983) Comparison of arterial wall mechanics using ring and cylindrical segments. Am J Physiol Heart Circ Physiol 244(2):H298–H303
3. Dignan RJ, Yeh T Jr, Dyke CM, Lutz HA III, Wechsler AS (1992) The influence of age and sex on human internal mammary artery size and reactivity. Ann Thorac Surg 53(5):792–797
4. Hoeltzel DA, Buzard K, K-i C, Altman P (1992) Strip extensiometry for comparison of the mechanical response of bovine, rabbit, and human corneas. J Biomech Eng 114(2):202–215
5. Sokolis D (2007) Passive mechanical properties and structure of the aorta: segmental analysis. Acta Physiol 190(4):277–289
6. Tanaka TT, Fung Y-C (1974) Elastic and inelastic properties of the canine aorta and their variation along the aortic tree. J Biomech 7(4):357–370
7. Y. Fung Biomechanics: mechanical properties of living tissues. 1993. Springer-Verlag, New York
8. Holzapfel GA, Sommer G, Gasser CT, Regitnig P (2005) Determination of layer-specific mechanical properties. Circulation 289:H2048–2058
9. Twal WO, Klatt SC, Harikrishnan K, Gerges E, Cooley MA, Trusk TC, Zhou B, Gabr MG, Shazly T, Lessner SM (2013) Cellularized microcarriers as adhesive building blocks for fabrication of tubular tissue constructs. Ann Biomed Eng 41:1–12
10. J. D. Humphrey (2002) Cardiovascular solid mechanics: cells, tissues, and organs. Springer,
11. Ingels N, Hansen DE, Daughters G, Stinson EB, Alderman EL, Miller DC (1989) Relation between longitudinal, circumferential, and oblique shortening and torsional deformation in the left ventricle of the transplanted human heart. Circ Res 64(5):915–927
12. McCULLOCH AD, Smaill BH, Hunter PJ (1987) Left ventricular epicardial deformation in isolated arrested dog heart. Am J Physiol Heart Circ Physiol 252(1):H233–H241
13. Pirolo J, Branham B, Creswell L, Perman W, Vannier M, Pasque M (1992) Pressure-gated acquisition of cardiac MR images. Radiology 183(2):487–492
14. Waldman LK, Fung Y, Covell JW (1985) Transmural myocardial deformation in the canine left ventricle. Normal *in vivo* three-dimensional finite strains. Circ Res 57(1):152–163
15. Bruck H, McNeill S, Sutton MA, Peters Iii W (1989) Digital image correlation using Newton–Raphson method of partial differential correction. Exp Mech 29(3):261–267
16. Chu T, Ranson W, Sutton M (1985) Applications of digital-image-correlation techniques to experimental mechanics. Exp Mech 25(3): 232–244
17. Luo P, Chao Y, Sutton M, Peters W III (1993) Accurate measurement of three-dimensional deformations in deformable and rigid bodies using computer vision. Exp Mech 33(2):123–132
18. Luo P-F, Chao YJ, Sutton MA (1994) Application of stereo vision to three-dimensional deformation analyses in fracture experiments. Opt Eng 33(3):981–990
19. H. Schreier, J-J. Orteu, M. A. Sutton (2009) Image correlation for shape, motion and deformation measurements: basic concepts, theory and applications. Springer-Verlag US
20. Sutton M, Mingqi C, Peters W, Chao Y, McNeill S (1986) Application of an optimized digital correlation method to planar deformation analysis. Image Vis Comput 4(3):143–150
21. Sutton M, Wolters W, Peters W, Ranson W, McNeill S (1983) Determination of displacements using an improved digital correlation method. Image Vis Comput 1(3):133–139
22. M. A. Sutton (2008) Digital image correlation for shape and deformation measurements. In: Springer handbook of experimental solid mechanics. Springer, pp 565–600
23. Ning J, Wang Y, Sutton MA, Anderson K, Bischoff JE, Lessner SM, Xu S (2010) Deformation measurements and material property estimation of mouse carotid artery using a microstructure-based constitutive model. J Biomech Eng 132(12):121010
24. Sutton M, Ke X, Lessner S, Goldbach M, Yost M, Zhao F, Schreier H (2008) Strain field measurements on mouse carotid arteries using microscopic three–dimensional digital image correlation. J Biomed Mater Res A 84(1):178–190
25. Kim J, Baek S (2011) Circumferential variations of mechanical behavior of the porcine thoracic aorta during the inflation test. J Biomech 44(10):1941–1947
26. Rv M (1945) On Saint Venant's principle. Bull Am Math Soc 51(8): 555–562
27. A. Green, W. Zerna Theoretical elasticity, 1954. Clarendon Press, Oxford
28. T. H. Elshazly (2004) Characterization of PVA hydrogels with regards to vascular graft development
29. A. Rachev, T. ElShazly, D. N. Ku Constitutive formulation of the mechanical properties of synthetic hydrogels. In: ASME 2004 International Mechanical Engineering Congress and Exposition, 2004. American Society of Mechanical Engineers, pp 353–354
30. Gasser TC, Ogden RW, Holzapfel GA (2006) Hyperelastic modelling of arterial layers with distributed collagen fibre orientations. J R Soc Interface 3(6):15–35
31. Holzapfel GA, Gasser TC, Ogden RW (2000) A new constitutive framework for arterial wall mechanics and a comparative study of material models. J Elast Phys Sci Solids 61(1–3):1–48
32. Gleason R, Humphrey J (2004) A mixture model of arterial growth and remodeling in hypertension: altered muscle tone and tissue turnover. J Vasc Res 41(4):352–363
33. Holzapfel GA, Gasser TC (2007) Computational stress-deformation analysis of arterial walls including high-pressure response. Int J Cardiol 116(1):78–85
34. Holzapfel GA (2006) Determination of material models for arterial walls from uniaxial extension tests and histological structure. J Theor Biol 238(2):290–302
35. L. Li, X. Qian, S. Yan, L. Hua, H. Zhang, Z. Liu (2012) Determination of the material parameters of four-fibre family model based on uniaxial extension data of arterial walls. Computer methods in biomechanics and biomedical engineering (ahead-of-print):1–9
36. Li L, Qian X, Yan S, Lei J, Wang X, Zhang H, Liu Z (2013) Determination of material parameters of the two-dimensional Holzapfel–Weizsäcker type model based on uniaxial extension data of arterial walls. Comput Methods Biomech Biomed Eng 16(4):358–367